Catena 74 (2008) 58–64

Contents lists available at ScienceDirect

Catena

journal homepage: www.elsevier.com/locate/catena

Reconstructing the paleotopography beneath the loess cover with the aid of an electromagnetic induction sensor

Timothy Saey [a,*], David Simpson [a], Udayakantha W.A. Vitharana [a], Hans Vermeersch [a], Jan Vermang [b], Marc Van Meirvenne [a]

[a] Research Group Soil Spatial Inventory Techniques, Department of Soil Management and Soil Care, Faculty of Bioscience Engineering, Ghent University, Coupure 653, B-9000 Gent, Belgium
[b] Laboratory of Soil Physics, Department of Soil Management and Soil Care, Faculty of Bioscience Engineering, Ghent University, Coupure 653, B-9000 Gent, Belgium

ARTICLE INFO

Article history:
Received 31 October 2007
Received in revised form 26 February 2008
Accepted 17 March 2008

Keywords:
EM38DD
Apparent electrical conductivity
Paleolandscape
Tertiary substrate
Quaternary loess cover
Erosion patterns

ABSTRACT

During the last glacial period (Weichselian), wind-blown loess was deposited over the undulating landscape of central Belgium, which had been formed in surfacing Tertiary marine sediments. Since valleys were filled up with a thicker loess layer than hill tops, the present topography is much smoother. This smoothing was enhanced by subsequent erosion processes. Reconstructing the paleolandscape at a detailed scale is almost impossible by conventional procedures based on soil augerings. Therefore, the use of the electromagnetic induction sensor, EM38DD, was evaluated as an alternative for mapping the depth to the Tertiary clay substrate. On our 2.7 ha study site, located in the loess belt of central Belgium, a strong non-linear relationship (R^2=0.86) was found between the apparent electrical conductivity (ECa), measured by the vertical dipole orientation of the EM38DD and the depth to a Tertiary clay substrate. These predictions were validated by independent observations of the depth to the Tertiary clay and a correlation coefficient of 0.83, with an average error of 0.22 m, was found. So, our dense ECa measurements (2 by 2 m resolution) allowed us to build a three-dimensionall surface of the depth to the Tertiary substrate, reconstructing the paleotopography beneath the loess cover. This paleotopography revealed distinct erosion patterns on the surface of the Tertiary clay. The continuity of these was confirmed by an analysis of surface flow patterns conducted on the reconstructed paleotopography. The non-invasive, time- and cost-effective electromagnetic induction sensor was found to offer new perspectives to reconstruct and analyse in detail the Quaternary paleotopography beneath the loess cover.

1. Introduction

The loess belt of Central Europe extends from the Atlantic coast, through central Belgium, to Eastern Europe. During the last glacial period (Weichselian), the periglacial undulating landscape of central Belgium had been formed in surfacing Tertiary marine sands and clays. This paleolandscape was covered by niveo-aeolian loess, with a thickness ranging from only a few decimeters on hill tops up to several tens of meters in valleys (Gillijns et al., 2005). As a consequence, the paleotopography was strongly smoothened and since slope processes have modified the thickness of the loess layer further, the paleotopography cannot be reconstructed on the basis of the present topography. The world's major loess deposits have correctly been linked to glacial processes or to cold weathering processes (Iriondo and Kröhling, 2007). Yet, a precise and accurate representation of landforms and niveo-aeolian loess sediments offers fundamental information about Pleistocene periglacial environments (Smith et al., 2006).

Geomorphological mapping, particularly at large scales (1:10 000 or greater) is one of the most important techniques in Quaternary research with the aim at analyzing glacial landscapes, including those resulting from the passage of the last ice sheets and particularly from more recent phases of glacier activity (Lowe and Walker, 1997). However, traditional geomorphological mapping needs to adapt to challenges for greater precision and objectivity within a GIS environment (Gustavsson et al., 2006). Leverington et al. (2002) digitally reconstructed late Quaternary landscapes by using a GIS method that subtracted interpolated isobase values from modern elevations. These maps served for the reconstruction of the Quaternary landscape on a large scale and with a limited accuracy. Therefore, quantifications of the subtle changes in paleotopography could not be made.

The extent to which conventional invasive methods can be employed for the quantification of the small-scale soil variability is often limited by the availability of expertise and the expense and labour associated with obtaining soil samples by augering (Stroh et al., 2001). Non-invasive geophysical methods (like seismic, geo-electric and electromagnetic) have proven to be effective for investigating the stratigraphy over relatively large depths (20–80 m) (Bersezio et al., 2007; Sass, 2007; Sloan et al., 2007). While geophysical investigations

* Corresponding author. Fax: +32 9 264 62 47.
E-mail address: Timothy.Saey@UGent.be (T. Saey).

0341-8162/$ – see front matter © 2008 Elsevier B.V. All rights reserved.
doi:10.1016/j.catena.2008.03.007

focus on the exploration of natural resources, hydrogeology or engineering purposes, knowledge about the applicability in shallow (<3 m) subsurface exploration for geomorphologic purposes is still incomplete (Sass, 2007). To investigate the soil constitution over shallower depths, soil-adapted geophysical sensors, like the EM38DD (Geonics Ltd., Mississauga, ON, Canada), have proved their functioning (Boll et al., 1996; Sudduth et al., 2003; Cockx et al., 2006; Cockx et al., 2007).

The objective of this study was to evaluate a methodology for mapping the paleotopography at shallow depths (<3 m) beneath the loess cover using the EM38DD electromagnetic induction (EMI) sensor. Therefore, a relationship between the paleotopography and the apparent electrical conductivity (ECa), measured by the EM38DD sensor, had to be found and validated. As a test case, a study site of 2.7 ha in central Belgium was used where the paleolandscape prior to the deposition of the loess cover was formed in Tertiary marine clay.

2. Materials and methods

2.1. Geology

The Belgian loess belt, which is part of the large European loess belt, is characterized by a gentle rolling landscape, where Tertiary marine sandy and clayey deposits were covered by a Quaternary loess layer (Vanwalleghem et al., 2005). Generally, the thickness of the loess cover varies with the position in the landscape. Thin loess deposits (sometimes as thin as a few decimetres) can be found on the ridges, while in depressions thick loess deposits (of several tens of meters) can occur. The main sedimentation phase of the Quaternary loess was in the Weichselian glacial stage of the Late Pleistocene (80 ka–10 ka) (Lowe and Walker, 1997).

The Tertiary material located directly below the Quaternary loess is composed of a range of marine depositions dating from the Early Eocene (54.8 Ma–49.0 Ma), generally with a clayey or sandy constitution. Within the study area this layer belongs to the clayey variant of the Ypresian (Maréchal and Laga, 1988).

2.2. Study site

The research site was located in Heestert (southeast of the province of West-Flanders, Belgium), situated in the Belgian loess belt (Fig. 1). It was situated on a southeast facing hillside with an average slope of 7% and an elevation ranging between 30 to 40 m above sea level (a.s.l.). The site consisted of two neighbouring fields. Field 1 was a 2 ha arable parcel (with central coordinates: 50°47′58”N, 3°24′41”E), planted to a sugar beet (*Beta vulgaris* L.)–winter wheat (*Triticum aestivum* L.) rotation. This field was used to calibrate and validate the relationship between ECa and the depth to the Tertiary substrate, observed after soil augering. Field 2 was a permanent pasture of 0.7 ha, located next to the eastern boundary of field 1 (with central coordinates: 50°47′01”N, 3°24′46”E). This field was added to reconstruct the paleotopography beyond the boundaries of the calibration field.

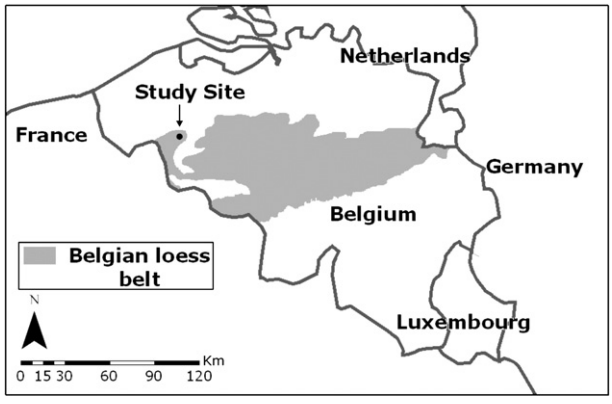

Fig. 1. Localization of the study site in the Belgian loess belt.

Table 1
Average textural composition of the Quaternary loess and Tertiary substrate based on samples taken along transect ABCD (*n*: number of samples, *m*: mean, *s*: standard deviation)

	n	Clay (%)		Silt (%)		Sand (%)	
		m	*s*	*m*	*s*	*m*	*s*
Quaternary loess	23	19.1	6.8	48.9	9.0	32.0	11.4
Tertiary substrate	17	40.2	8.0	53.3	7.2	6.5	5.6

On the national soil map (scale 1:20 000) one dominant soil series (uLdc) is indicated for both fields. These symbols represent: a shallow (<75 cm) clay substrate (u), a silt loam topsoil texture (L), moderately wet conditions (d) with a strongly degraded textural B-horizon (c). In the southern part of field 1 the shallow clay substrate was not indicated. This soil type corresponds to a Luvisol (WRB), which is characterized by an argic horizon ranging from 0.3–0.35 m up to 1.3–1.4 m in depth. Initially, the deposited loess was calcareous, but with time it decalcified, mostly down to a depth of 2–2.5 m (Hubert, 1976).

Across the study site, soil samples were taken from the Quaternary loess and the Tertiary clay substrate and analyzed for their textural composition according to the conventional sieve-pipette method. The mean clay-silt-sand fractions (with boundaries 2–50–2000 μm, respectively) of both the 23 Quaternary and the 17 Tertiary samples are given in Table 1, together with their standard deviations. On average, the loess layer has a larger sand content (32.0%) and a lower clay content (19.1%) than the Tertiary material (6.5% sand and 40.2% clay). Both layers show a relatively limited variability in soil texture, but the Tertiary clay layer is more homogeneous than the loess. These differences illustrate the relative easiness for an experienced soil scientist to distinguish between both layers in the field.

2.3. Mobile ECa-measurement equipment and temperature standardization procedure

An EM38DD sensor was mounted on a sled pulled by an all terrain vehicle (ATV), which drove with a speed of 6–10 km h^{-1} (Fig. 2(a) and (b)). The EM38DD is a dual dipole sensor and consists of two single EM38′s positioned perpendicular to each other, with one instrument oriented horizontally and the other vertically. The EM38DD simultaneously measures the ECa in the two dipole orientations: vertical (ECa_v) and horizontal (ECa_h). Every second, ECa_v and ECa_h measurements were recorded by a field computer. A Trimble AgGPS332, with Omnistar correction, was used to georeference the ECa measurements with a pass-to-pass accuracy of approximately 0.10 m. Measurements were taken along parallel lines with an in-between distance of 2 m, driving was supported by a Trimble Lightbar Guidance System. Additionally, at each ECa measurement point, the soil surface elevation was acquired with the Trimble AgGPS332 (accuracy ± 0.30 m). The ECa measurements on field 1 were taken on 27/04/2007; field 2 was surveyed on 19/06/2007. In both cases weather conditions were dry.

Since ECa measurements depend on the soil temperature, it is necessary to standardize them according to a reference temperature (Sheets and Hendrickx, 1995). Usually a reference temperature of 25 °C is taken (Slavich and Petterson, 1990):

$$ECa_{25} = ECa \cdot \left(0.447 + 1.4034 \cdot e^{-\frac{T}{26.815}}\right) \quad (1)$$

with ECa_{25} the standardized ECa at a temperature of 25 °C and T the soil temperature in °C. At the measurement dates, soil temperature was continuously measured at a depth of 0.20 m below soil surface, averaged and applied in Eq. (1). The ECa values presented in the

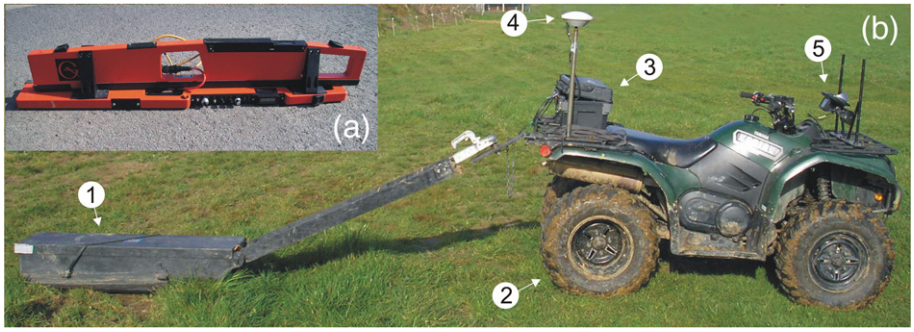

Fig. 2. EM38DD (a) and Mobile ECa-measurement equipment (b); 1: Sled with EM38DD, 2: All Terrain Vehicle, 3: Trimble AgGPS332 and field computer, 4: GPS antenna, 5: Lightbar Guidance System.

remaining part of this paper were all converted to a standard temperature of 25 °C.

2.4. Electromagnetic induction sensing

In EMI sensors, an alternating current is passed through a transmitter coil, which produces a primary magnetic field (H_p). This primary magnetic field induces eddy currents in the soil. These induced currents create a secondary magnetic field (H_s) proportional to the strength of the currents. The secondary magnetic field induces again alternating currents in the receiver coil, which is directly related to a depth-weighted average ECa (mS m^{-1}) (McNeill, 1980b):

$$\mathrm{ECa} = \frac{4}{2 \cdot \pi \cdot f \cdot \mu_0 \cdot s^2}\left(\frac{H_s}{H_p}\right) \tag{2}$$

With f the frequency (Hz), μ_0 the permeability of free space ($4\pi \times 10^{-7}$ H m^{-1}), s the intercoil spacing (m) which is 1 m for the EM38DD, H_s the secondary magnetic field at the receiver coil (H m^{-1}), and H_p the primary magnetic field at the transmitter coil (H m^{-1}). The major advantages of EMI are: (i) it is non-invasive; (ii) it gives an immediate response; (iii) the signal has a good penetration capacity in porous media; and (iv) the signal response can be related to soil composition (Cockx et al., 2006).

The EM38DD EMI instrument measures the ECa in the two orientations, each having a different depth response profile. The vertical dipole orientation receives a dominant influence from deeper (0.3–0.6 m) soil layers, while the horizontal orientation receives its major influence from near-surface (0–0.3 m) soil layers. The cumulative EM38-response (expressed in % of the measured signal) from the soil volume below a depth z (in m) was given by McNeill (1980b), both for the vertical ($R_v(z)$) and the horizontal orientations ($R_h(z)$):

$$R_v(z) = \left(4 \cdot z^2 + 1\right)^{-0.5} \tag{3}$$

$$R_h(z) = \left(4 \cdot z^2 + 1\right)^{0.5} - 2 \cdot z \tag{4}$$

From these it can be deduced that the soil volume below 1.60 m depth for $R_v(z)$ and below 0.75 m depth for $R_h(z)$ yields a contribution of 30% in the measured signal, or 70% of the measured signal comes from the soil volume above these 1.60 m and 0.75 m depths respectively. The $\mathrm{ECa_v}$ and $\mathrm{ECa_h}$ measurements can be combined in the profile ratio (PR) which provides an indication of the heterogeneity of the soil profile:

$$\mathrm{PR} = \mathrm{ECa_h}/\mathrm{ECa_v}. \tag{5}$$

In a two-layered model where silty soil (like loess) is located above clayey material, the relationship between the depth to the clay substrate (z_{clay}) and the $\mathrm{ECa_v}$ can be modelled by using the McNeill (1980b) cumulative response $R_v(z_{clay})$ from the soil below z_{clay} (Eq. (3)). The cumulative response from the upper Quaternary loess and the lower Tertiary clayey material can be calculated as $1 - R_v(z_{clay})$ and $R_v(z_{clay})$, respectively. Therefore, at each z_{clay}, the corresponding $\mathrm{ECa_v^*}$ can be modelled given the apparent conductivity values of homogeneous Quaternary loess ($\mathrm{ECa_{v,loess}}$) and Tertiary clay ($\mathrm{ECa_{v,clay}}$):

$$\mathrm{ECa_v^*} = \left[1 - R_v\left(z_{clay}\right)\right] \cdot \mathrm{ECa_{v,loess}} + \left[R_v\left(z_{clay}\right)\right] \cdot \mathrm{ECa_{v,clay}} \tag{6}$$

Inversely, z^*_{clay} can be modelled given the $\mathrm{ECa_v}$ measurements. Therefore, $R_v(z^*_{clay})$ was calculated given the $\mathrm{ECa_v}$ measurements, $\mathrm{ECa_{v,loess}}$ and $\mathrm{ECa_{v,clay}}$:

$$R_v\left(z^*_{clay}\right) = \frac{\mathrm{ECa_v} - \mathrm{ECa_{v,loess}}}{\mathrm{ECa_{v,clay}} - \mathrm{ECa_{v,loess}}}. \tag{7}$$

This calculated $R_v(z^*_{clay})$ can be input to Eq. (3) to obtain the modelled z^*_{clay}:

$$z^*_{clay} = \left[\frac{1}{4 \cdot R_v\left(z^*_{clay}\right)^2} - \frac{1}{4}\right]^{0.5} \tag{8}$$

To fit a theoretical relationship to the z_{clay}–$\mathrm{ECa_v}$ data points based on the McNeill (1980b) cumulative depth response, the sum of the squared differences between z_{clay} and z^*_{clay} must be minimized:

$$\sum_{i=1}^{n}\left[z_{clay}(i) - z^*_{clay}(i)\right]^2 = \min \tag{9}$$

with i the number of the observation and n the total amount of observations. z^*_{clay} was modelled with Eqs. (7) and (8) given the $\mathrm{ECa_v}$ measurements. The modelling parameters $\mathrm{ECa_{v,loess}}$ and $\mathrm{ECa_{v,clay}}$ were iteratively adjusted to obtain the smallest sum of the squared differences between z_{clay} and z^*_{clay}.

A similar approach can be followed to fit the theoretical relationship according to McNeill (1980b) to the z_{clay}–$\mathrm{ECa_h}$ data given the cumulative response $R_h(z_{clay})$ from the soil below a depth of z_{clay} (Eq. (4)).

With the low-frequency EM38DD sensor, high-resolution ECa measurements can be achieved in a cost- and labour-effective way. Soil ECa relates to a number of soil properties, including soil porosity, soil moisture content, concentration of dissolved electrolytes in the soil water, soil temperature and the amount and composition of colloids (McNeill, 1980a). In non-saline soils, like at the study site, ECa reflects mainly differences in clay and moisture content (Domsch and Giebel, 2004; McBratney et al., 2005). This makes the ECa measurements appropriate to account for differences in depth to clay layers (Doolittle et al., 1994; Sudduth et al., 2003; Cockx et al., 2007) based on the conductivity contrasts between topsoil and subsoil material.

After modelling z^*_{clay} given the ECa measurements, an independent validation can be executed to evaluate the model performance. Three

validation indices were used as validation criteria: the mean estimation error (MEE), the root mean-squared estimation error (RMSEE) and the Pearson correlation coefficient r. The MEE and RMSEE were obtained from:

$$\mathrm{MEE} = \frac{1}{n}\sum_{i=1}^{n}\left[z^{*}_{\mathrm{clay}}(i) - z_{\mathrm{clay}}(i)\right] \tag{10}$$

$$\mathrm{RMSEE} = \sqrt{\frac{1}{n}\sum_{i=1}^{n}\left[z^{*}_{\mathrm{clay}}(i) - z_{\mathrm{clay}}(i)\right]^{2}} \tag{11}$$

with i the number of the validation observation and n the total amount of validation observations. The MEE and RMSEE values are measures of the bias and accuracy respectively. They should approach zero as the model predictions become optimal. An r value close to one indicates a strong positive linear relationship between observed and predicted depths.

2.5. Interpolation and validation indices

In order to obtain estimates of variables at unsampled locations, ordinary point kriging (OK) was used as interpolation method. OK provides estimates of a variable at any unsampled location using a linear combination of observations within a predefined neighbourhood around this location (Goovaerts, 1997). In this study, a maximum of 8 neighbours were used within a circular search area with a radius of 10 m around the location being interpolated. The spatial structure of the variables was represented by variogram models, which were used to assign weights to these neighbours. With the contouring and 3D surface mapping program Surfer (Golden Software Inc., Golden, CO, U.S.A.), theoretical variogram models were manually fit to the experimental variograms. Gaussian variogram models with a nugget variance (C_0) were found to represent the experimental variograms best; these models are defined as follows:

$$\gamma(h) = \begin{cases} 0 & \text{if } h = 0 \\ C_0 + C_1 \cdot \left[1 - \exp\left(-\dfrac{3h^2}{a^2}\right)\right] & \text{if } 0 < h \le a \\ C_0 + C_1 & \text{if } h > a \end{cases} \tag{12}$$

with $\gamma(h)$ the semivariance at lag distances h, C_1 the sill and a the range. Finally, maps with a pixel resolution of 0.5 by 0.5 m were obtained after OK.

3. Results and discussion

3.1. ECa mapping

Table 2 shows the summary statistics of the EM38DD measurements for both fields. The mean of the ECa_v measurements of both fields (91 mS m^{-1}) was much larger compared to the ECa_h measurements (48 mS m^{-1}). As a consequence, the average PR was distinctively smaller than 1. This indicates that, in general, higher conductive soil is located below less conductive material. The standard deviations were the largest for field 1, indicating that this field was more heterogeneous in soil composition.

Table 2
Descriptive statistics (m: mean, min: minimum, max: maximum, s: standard deviation) of ECa_v, ECa_h and PR for the two fields (field 1 contained 5509 measurement points, field 2 contained 1814 measurement points)

Variable	Field 1				Field 2			
	m	min	max	s	m	min	max	s
ECa_v (mS m^{-1})	91	49	144	21	91	68	110	11
ECa_h (mS m^{-1})	48	19	100	15	48	32	72	7
PR	0.51	0.34	1.17	0.05	0.53	0.44	0.76	0.03

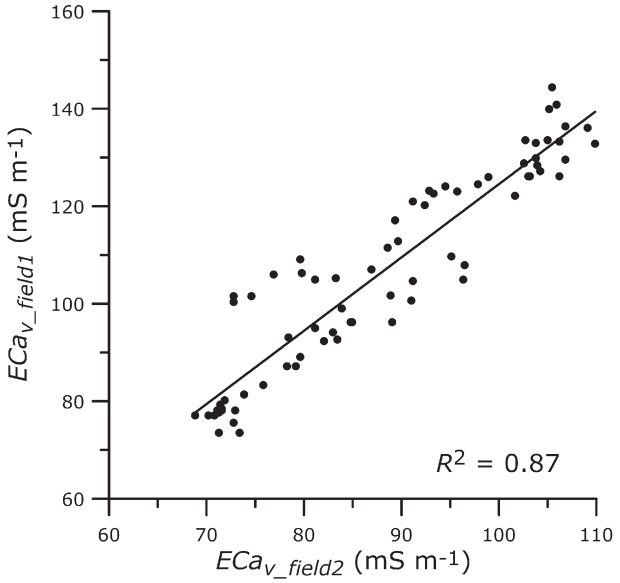

Fig. 3. ECa_{v_field1} as a function of ECa_{v_field2} (72 data points at the boundary of both fields).

Since the absolute values of ECa measured under different cultivation or soil moisture conditions could not be compared directly, measurements (already standardized at 25 °C) of adjacent fields had to be rescaled to a common basis. Therefore the ECa values located near to the boundary between field 1 and field 2 were matched using a nearest neighbour search within a moving window with a radius of 7 m centred at each point of field 2. The ECa_v of pairs of neighbours located in the opposite field were plotted in Fig. 3 and the following linear regression was fit to them:

$$\mathrm{ECa}_{\mathrm{v\_field1}} = 1.50 \cdot \mathrm{ECa}_{\mathrm{v\_field2}} - 25.85 \qquad R^2 = 0.87 \tag{13}$$

Using this relationship, ECa values of the entire second field were converted to a common basis with field 1 and these data were used in the remainder of this paper.

The ECa_v measurements of both fields were interpolated as shown in Fig. 4. The variogram parameters are defined in Table 3. It can be

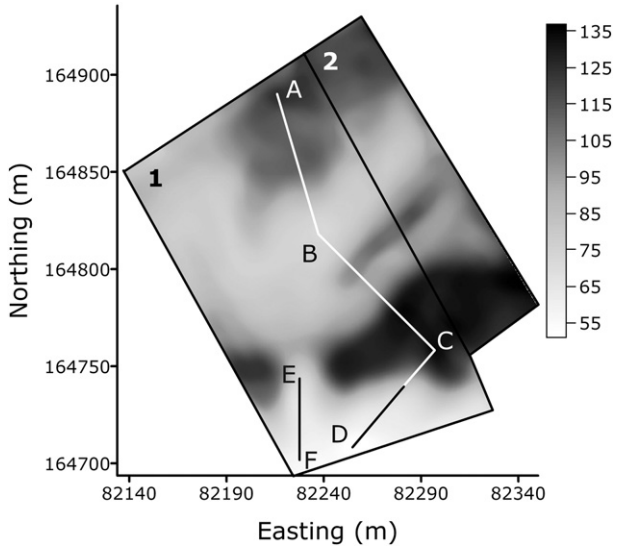

Fig. 4. Map of interpolated ECa_v (mS m^{-1}) with transects ABCD and EF.

Table 3
Parameters of the Gaussian variogram model for ECa_v, Z, $Z-z^*_{clay}$ and z^*_{clay} (C_0: nugget variance; C_1: sill and a: range)

Variable	C_0	C_1	a (m)
ECa_v (mS m^{-1})	5	446	29
Z (m)	0.0	7.7	129
$Z-z^*_{clay}$ (m)	0.005	23.005	150
z^*_{clay} (m)	0.003	0.353	30

seen that the highest ECa values occurred in the northern and in the southeastern parts of the study area. Moreover, the conversion to a common basis of the measurements of both fields resulted in a close match and a continuity beyond the boundary between both fields.

3.2. Depth to tertiary clay observations

Two transects ABCD and EF were laid out in such a way that both the largest and lowest ECa measurements of field 1 were visited equally (Fig. 4). Along the 225 m of transect ABCD 46 observation points were located at 5 m intervals, while along the 42 m of transect EF 15 points were selected at 3 m intervals. At each of these 61 points, z_{clay} was observed by augering with a gouge auger.

Fig. 5(b) shows z_{clay} in respect to elevation together with the present day soil surface for transect ABCD. At most locations, a clearly observable distinction was present between the loess topsoil and the Tertiary clay. However, between points B and C, a mixture of loess-clay was found on top of the clayey substrate at some locations. This mixture was maximally about 0.5–0.6 m thick. Along this transect, the Tertiary clay substrate was present within the first 1.6 m at the first 42 sampling points. The last four sampling points on transect ABCD were characterized by a loess layer that extended down to more than 3.5 m, which was the maximal augering depth. At 14 observation points along transect EF, the Tertiary substrate was located between 1.5 and 3 m below the soil surface. The exact z_{clay} of the remaining sampling point was unavailable, due to the extent of the loess cover below the 3.5 m boundary.

3.3. Relationship between ECa and depth to tertiary clay

Fig. 5(a) shows the ECa_v and ECa_h profiles measured along the transect ABCD. It is clear that these profiles behave similarly to the depth to Tertiary clay as shown in Fig. 5(b). The 42 z_{clay} observations of transect ABCD and the 14 observations of transect EF were compared with their nearest ECa measurements. The fitting of the McNeill-relationship to the $z_{clay}-ECa_v$ data points was done by minimizing the sum of the squared differences between z_{clay} and z^*_{clay} by iteratively altering the modelling parameters $ECa_{v,loess}$ and $ECa_{v,clay}$ in Eqs. (7) and (8). The optimal values of $ECa_{v,loess}$ and $ECa_{v,clay}$ were 36 and 150 mS m^{-1}, respectively, with a R^2 of 0.86 (Fig. 6). The same procedure was applied to the $z_{clay}-ECa_h$ data. The resulting $ECa_{h,loess}$ and $ECa_{h,clay}$ were 12 and 145 mS m^{-1}, respectively, with a R^2 of 0.88. However, as the theoretical relationship by McNeill (1980b) indicates, the horizontal orientation is less sensitive to deeper soil layers. It receives 70% of its influence from the top 0.75 m in homogeneous soil while the vertical orientation integrates 70% of its response over the

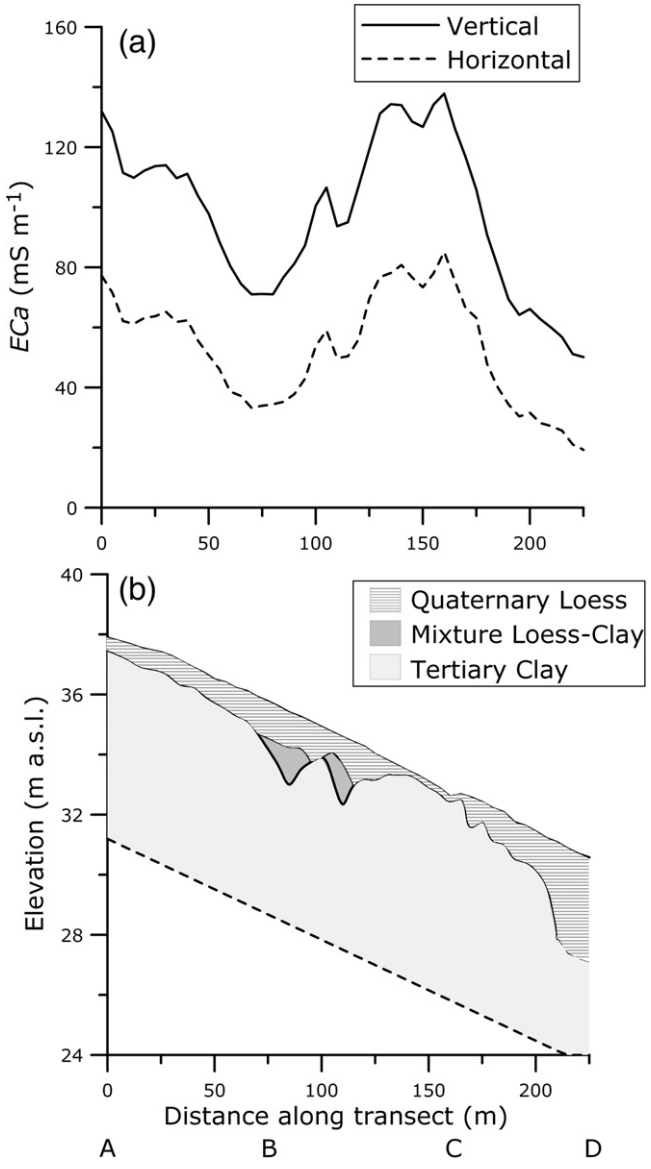

Fig. 5. ECa_v and ECa_h measurements along the 225 m transect ABCD (a) and the build up of the three layers encountered along this transect (b).

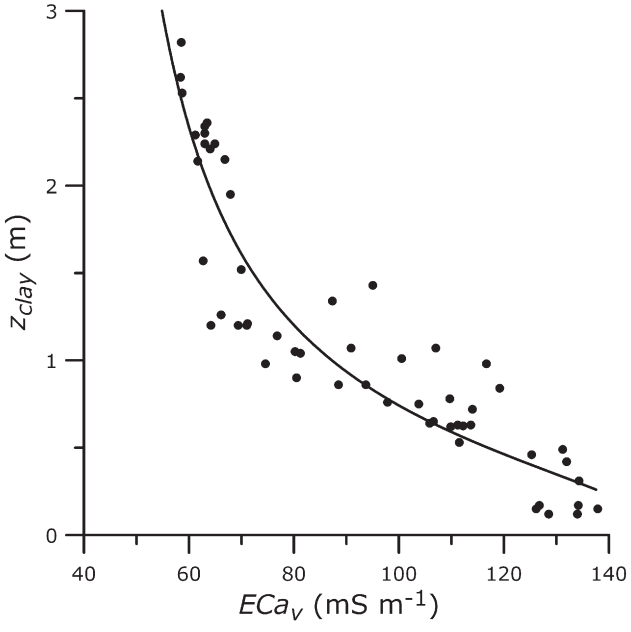

Fig. 6. z_{clay} as a function of ECa_v along study transects ABCD and EF with fitted McNeill-curve.

top 1.60 m soil. Therefore preference was given to the z_{clay}–ECa_v relationship to model z^*_{clay}:

$$z^*_{clay} = \left[\frac{1}{4\cdot\left(\frac{ECa_v-36}{114}\right)^2}-\frac{1}{4}\right]^{0.5} \quad (14)$$

3.4. Validation of predicted depth of tertiary clay

The accuracy of the proposed model to predict z^*_{clay} was evaluated by investigating at 24 locations, laid out as a grid. At these locations, the observed depths were compared with the modelled depths. The MEE and RMSEE were respectively 0.04 m and 0.22 m. The r between z_{clay} and z^*_{clay} was 0.83 (Fig. 7). Therefore, the modelled relationship had a low bias, was reasonably accurate and correlated well with the observed depths.

3.5. Paleotopography beneath the loess cover

The soil surface elevation (Z) of the fields was interpolated and visualized in Fig. 8(a). The ECa_v measurements were converted into z^*_{clay} using Eq. (14). We did not use an interpolation method, like regression kriging or simple kriging with varying local means (Goovaerts, 1997), to construct the z^*_{clay} map because the spatial configuration of the observations of z_{clay} was concentrated along one transect only. The predicted z^*_{clay} were subtracted from Z and the resulting $Z-z^*_{clay}$ values were interpolated as shown in Fig. 8(b). To improve the visibility of the paleotopography, the interpolated map of z^*_{clay} is displayed in Fig. 8(c). The previous interpolations were carried out based on the variogram parameters given in Table 3. When comparing the current topography (Fig. 8(a)) with the paleotopography represented by the Tertiary clay (Fig. 8(b) and (c)), it will be clear that the paleolandscape beneath the loess cover is less smooth. A pattern of shallow gullies emerged in the Tertiary substrate, despite its clayey composition. These gullies combine into one major gully which ends in what seems to be a wider valley. To evaluate the continuity of these flow pathways, the Idrisi Kilimanjaro (Clark Labs, Worcester, MA, U.S.A.) modules RUNOFF (Jenson and Domingue, 1988) and

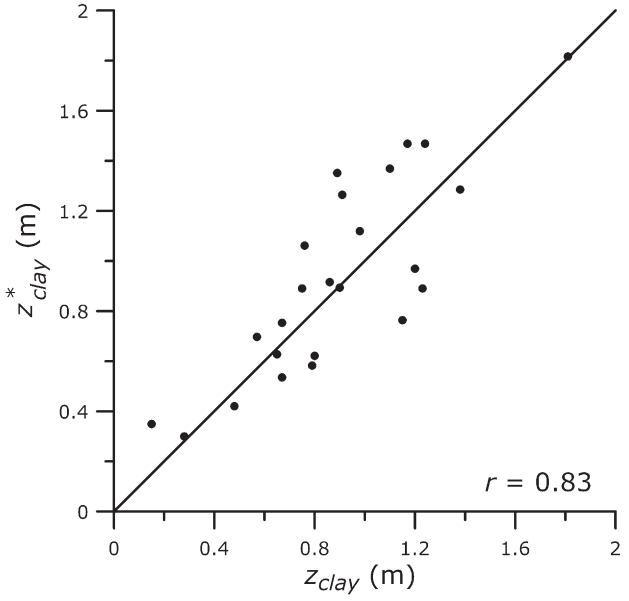

Fig. 7. Validation of predicted depth to the Tertiary clay (z^*_{clay}) using 24 observed depths (z_{clay}).

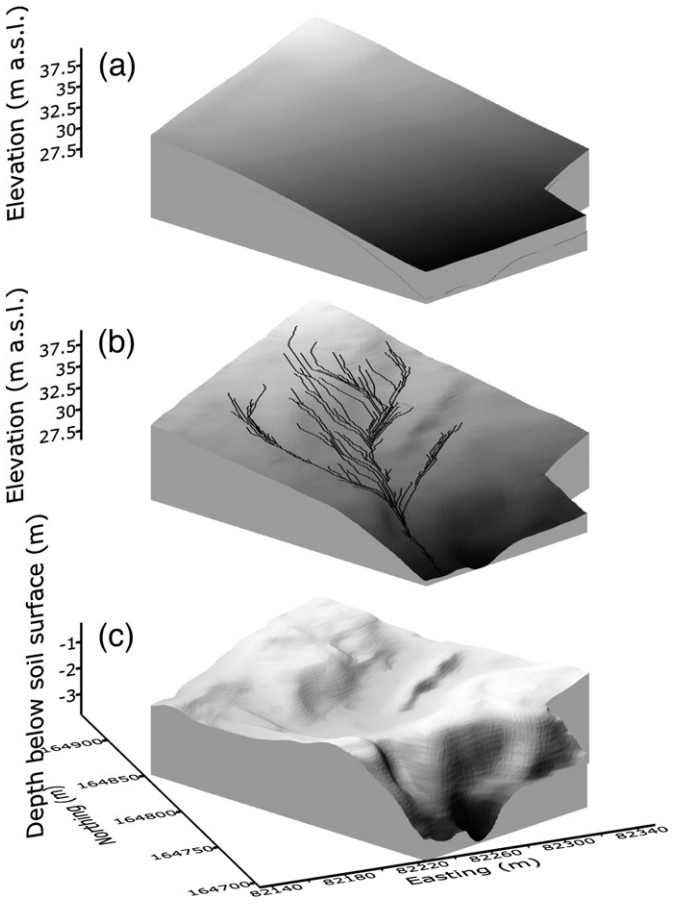

Fig. 8. Current soil surface (a), paleotopography beneath the loess cover represented as elevation above sea level with indications of simulated flow lines (b), and paleotopography represented as depth below soil surface (c).

WATERSHED were applied to the paleotopography surface. The result is visualized in Fig. 8(b). A clear accumulation of flow lines, representing past surface flow patterns, emerges. Hubert (1976) reported the occurrence of strong erosion during the glacial stages of the Pleistocene. Due to the deposition of the wind transported loess in the Late-Pleistocene the variability of the glacial Quaternary surface disappeared, however, locally a mixture of loess and clay remained, as observed between point B and C on the transect (Fig. 5(b)). Valleys were filled up with thick loess sediments, while elevated locations were covered by a thin layer. Subsequent erosion modified the thickness of the loess further, increasing the thickness of the valley loess by colluvial deposits.

4. Conclusions

The ECa measurements of the EM38DD sensor in the vertical mode proved to be suitable to predict z_{clay}. The relationship between z_{clay} and ECa was found to be best represented by the theoretical response curve proposed by McNeill (1980b). Also, measurements obtained on one field could be combined with those of an adjacent field without the need of additional field validation. The reconstructed paleotopography showed realistic patterns of surface processes, which could be modelled as a continuous flow process by a flow runoff model.

As a result, we can conclude that the combination of high density EMI sensor measurements with direct observations of the depth of the Tertiary clay beneath the Quaternary loess cover for shallow depths (<3 m), proved to be a successful method for the reconstruction of the paleotopography at the end of the last glacial period.

Acknowledgements

This research was supported by the Fund for Scientific Research-Flanders (FWO-Vlaanderen). The authors thank Mr. M. Coussement for granting access to his fields to carry out this study and Mr. M. Schatteman and Mr. L. Deboosere for their help with the laboratory analysis.

References

Bersezio, R., Giudici, M., Mele, M., 2007. Combining sedimentological and geophysical data for high-resolution 3-D mapping of fluvial architectural elements in the Quaternary Po plain (Italy). Sedimentary Geology 202, 230–248.

Boll, J., van Rijn, R.P.G., Weiler, K.W., Ewen, J.A., Daliparthy, J., Herbert, S.J., Steenhuis, T.S., 1996. Using ground-penetrating radar to detect layers in a sandy field soil. Geoderma 70, 117–132.

Cockx, L., Ghysels, G., Van Meirvenne, M., Heyse, I., 2006. Prospecting frost-wedge pseudomorphs and their polygonal network using the electromagnetic induction sensor EM38DD. Permafrost and Periglacial Processes 17, 163–168.

Cockx, L., Van Meirvenne, M., De Vos, B., 2007. Using the EM38DD soil sensor to delineate clay lenses in a sandy forest soil. Soil Science Society of America Journal 71, 1314–1322.

Domsch, H., Giebel, A., 2004. Estimation of soil textural features from soil electrical conductivity recorded using the EM38. Precision Agriculture 5, 389–409.

Doolittle, J.A., Sudduth, K.A., Kitchen, N.R., Indorante, S.J., 1994. Estimating depth to clays using electromagnetic induction methods. Journal of Soil and Water Conservation 49, 572–575.

Gillijns, K., Poesen, J., Deckers, J., 2005. On the characteristics and origin of closed depressions in loess-derived soils in Europe — a case study from central Belgium. Catena 60, 43–58.

Goovaerts, P., 1997. Geostatistics for Natural Resources Evaluation. Oxford University Press, New York.

Gustavsson, M., Kolstrup, E., Seijmonsbergen, A.C., 2006. A new symbol-and-GIS based detailed geomorphological mapping system: renewal of a scientific discipline for understanding landscape development. Geomorphology 77, 90–111.

Hubert, P., 1976. Verklarende tekst bij het kaartblad: Zwevegem 97E. Hoste-Staelens, Gent.

Iriondo, M.H., Kröhling, D.M., 2007. Non-classical types of loess. Sedimentary Geology 202, 352–368.

Jenson, S., Domingue, J., 1988. Extracting topographic structure from digital elevation data for geographic information system analysis. Photogrammetric Engineering and Remote Sensing 54, 1593–1600.

Leverington, D.W., Teller, J.T., Mann, J.D., 2002. A GIS method for reconstruction of late Quaternary landscapes from isobase data and modern topography. Computers and Geosciences 28, 631–639.

Lowe, J.J., Walker, M.J.C., 1997. Reconstructing Quaternary environments. Pearson Education Limited, Essex.

Maréchal, R., Laga, P., 1988. Voorstel lithostratigraphische indeling van het Paleogeen. Commissie Tertiair. Nationale Commissie voor Stratigrafie, Brussel.

McBratney, A., Minasny, B., Whelan, B.M., 2005. Obtaining 'useful' high-resolution soil data from proximally-sensed electrical conductivity/resistivity (PSEC/R) surveys. In: Stafford, J.V. (Ed.), Precision agriculture '05. Wageningen Academic Publishers, Wageningen, The Netherlands, pp. 503–510.

McNeill, J.D., 1980a. Electrical conductivity of soils and rocks. Technical Note TN-5. Geonics Limited, Missisauga, ON, Canada.

McNeill, J.D., 1980b. Electromagnetic terrain conductivity measurement at low induction numbers. Technical Note TN-6. Geonics Limited, Missisauga, ON, Canada.

Sass, O., 2007. Bedrock detection and talus thickness assessment in the European Alps using geophysical methods. Journal of Applied Geophysics 62, 254–269.

Sheets, K.R., Hendrickx, J.M.H., 1995. Non-invasive soil water content measurement using electromagnetic induction. Water Resources Research 31, 2401–2409.

Slavich, P.G., Petterson, G.H., 1990. Estimating average rootzone salinity for electromagnetic (EM-38) measurements. Australian Journal of Soil Research 28, 453–463.

Sloan, S.D., Tsoflias, G.P., Steeples, D.W., Vincent, P.D., 2007. High-resolution ultra-shallow subsurface imaging by integrating near-surface seismic reflection and ground-penetrating radar data in the depth domain. Journal of Applied Geophysics 62, 281–286.

Smith, M.J., Rose, J., Booth, S., 2006. Geomorphological mapping of glacial landforms from remotely sensed data: an evaluation of the principal data sources and an assessment of their quality. Geomorphology 76, 148–165.

Stroh, J.C., Archer, S., Doolittle, J.A., Wilding, L., 2001. Detection of edaphic discontinuities with ground-penetrating radar and electromagnetic induction. Landscape ecology 16, 377–390.

Sudduth, K.A., Kitchen, N.R., Bollero, G.A., Bullock, D.G., Wiebold, W.J., 2003. Comparison of electromagnetic induction and direct sensing of soil electrical conductivity. Agronomy Journal 95, 472–482.

Vanwalleghem, T., Poesen, J., Nachtergaele, J., Verstraeten, G., 2005. Characteristics, controlling factors and importance of deep gullies under cropland on loess-derived soils. Geomorphology 69, 76–91.